NOTES AND CORRESPONDENCE

Stability-Dependent Exchange Coefficients for Air–Sea Fluxes*

A. BIROL KARA, HARLEY E. HURLBURT, AND ALAN J. WALLCRAFT

Naval Research Laboratory, Stennis Space Center, Mississippi

(Manuscript received 8 January 2004, in final form 27 October 2004)

ABSTRACT

This study introduces exchange coefficients for wind stress (C_D), latent heat flux (C_L), and sensible heat flux (C_S) over the global ocean. They are obtained from the state-of-the-art Coupled Ocean–Atmosphere Response Experiment (COARE) bulk algorithm (version 3.0). Using the exchange coefficients from this bulk scheme, C_D, C_L, and C_S are then expressed as simple polynomial functions of air–sea temperature difference ($T_a - T_s$)—where air temperature (T_a) is at 10 m, wind speed (V_a) is at 10 m, and relative humidity (RH) is at the air–sea interface—to parameterize stability. The advantage of using polynomial-based exchange coefficients is that they do not require any iterations for stability. In addition, they agree with results from the COARE algorithm but at ≈5 times lower computation cost, an advantage that is particularly needed for ocean general circulation models (OGCMs) and climate models running at high horizontal resolution and short time steps. The effects of any water vapor flux in calculating the exchange coefficients are taken into account in the polynomial functions, a feature that is especially important at low wind speeds (e.g., $V_a < 5$ m s^{-1}) because air–sea mixing ratio difference can have a major effect on the stability, particularly in tropical regions. Analyses of exchange coefficients demonstrate the fact that water vapor can have substantial impact on air–sea exchange coefficients at low wind speeds. An example application of the exchange coefficients from the polynomial approach is the recalculation of climatological mean wind stress magnitude from 40-yr European Centre for Medium-Range Weather Forecasts (ECMWF) Re-Analysis (ERA-40) data in the North Pacific Ocean over 1979–2002. Using ECMWF 10-m winds and the authors' methodology provides accurate surface stresses while largely eliminating the orographically induced Gibb's waves found in the original ERA-40 surface wind stresses. These can have a large amplitude near mountainous regions and can extend far into the ocean interior. This study introduces exchange coefficients of air–sea fluxes, which are applicable to the wide range of conditions occurring over the global ocean, including the air–sea stability differences across the Gulf Stream and Kuroshio, regions which have been the subject of many climate model studies. This versatility results because C_D, C_L, and C_S are determined for V_a values of 1 to 40 m s^{-1}, ($T_a - T_s$), intervals of −8° to 7°C, and RH values of 0% to 100%. Exchange coefficients presented here are called the Naval Research Laboratory (NRL) Air–Sea Exchange Coefficients (NASEC) and they are suitable for a wide range of air–sea interaction studies and model applications.

1. Introduction

Previously, Kara et al. (2000, 2002) introduced polynomial functions for determining the exchange coefficients of wind stress (C_D), latent heat flux (C_L), and sensible heat flux (C_S) used in the bulk formulas. In these algorithms, the stability correction was approximated by a term depending on the sea–air temperature difference ($T_s - T_a$), where T_a is at 10 m, and a second-order polynomial function of the wind speed at 10 m above the sea surface (V_a) for C_D or the inverse wind speed for C_L. The algorithms do not require iteration to account for stability; therefore, they are computationally efficient for use in high-resolution coupled atmosphere–ocean circulation models and ocean general circulation models (OGCMs). They are also useful when,

* Naval Research Laboratory Contribution Number NRL/JA/7304/03/53.

Corresponding author address: Birol Kara, Naval Research Laboratory, Code 7320, Bldg. 1009, Stennis Space Center, MS 39529-5004.
E-mail: kara@nrlssc.navy.mil

© 2005 American Meteorological Society

every model time step, latent and sensible heat are calculated via the bulk formulas using both ocean model sea surface temperature (SST) and the high-frequency (e.g., 6-hourly or daily) wind speeds. This approach keeps model SST on track without any explicit relaxation to SST data or a climatology (e.g., Wallcraft et al. 2003).

The algorithms presented in the two studies mentioned above were obtained using tabulated exchange coefficients, which were published by Bunker (1976) and Isemer et al. (1989). The use of these two datasets resulted in a few limitations in the algorithms. For example, the datasets did not provide realistic exchange coefficients at high and low wind speeds, predominantly to allow for the biases inherent in estimating fluxes from ship observations. Many later studies indicated lower values for the exchange coefficients (e.g., DeCosmo et al. 1996; Yelland et al. 1998, 2002), in general. As a result, the algorithms based on these two sets usually resulted in errors (5%–25%) in estimating the wind stress and latent and sensible heat fluxes in comparison to those obtained from the standard Coupled Ocean–Atmosphere Response Experiment (COARE) version-2.5b (v2.5b) algorithm (Fairall et al. 1996). The COARE v2.5b algorithm determines the turbulent air–sea fluxes through a recursive solution for the atmospheric dynamic stability. However, this algorithm also has some deficiencies because it was only verified for winds up to 12 m s^{-1}. It is also noted that when Kara et al. (2000) was published and Kara et al. (2002) was under review, the COARE v2.5b algorithm was the accepted standard for air–sea flux estimates in the peer-reviewed scientific literature.

Fairall et al. (2003) later developed a new version of the COARE algorithm (v2.6 in 2001, renamed as v3.0 in 2003) with the aim of providing more realistic exchange coefficients at higher wind speeds based on the data collected since the release of COARE v2.5b. The new algorithm also takes additional observational data (Yelland et al. 1998; Hare et al. 1999) into account, which suggests that a Charnock constant value of 0.011 (Smith 1988), used in the earlier COARE v2.5b algorithm, is too low for higher wind speeds. Thus, a linear increase in the Charnock parameter is introduced between 10 and 18 m s^{-1} and a value of 0.018 is used for $\geq$18 m s^{-1} (Fairall et al. 2003). This might overestimate the roughness at very high wind speeds where Taylor and Yelland (2001) predict a decrease in the Charnock parameter.

With the availability of the improved COARE algorithm v3.0 (Fairall et al. 2003), it is now possible to obtain more realistic C_D and C_L values. This would reduce the uncertainties in the datasets ($\approx$10%–20%) used for deriving the exchange coefficients presented in Kara et al. (2000, 2002). In addition, the use of the COARE v3.0 has the advantage of providing reliable transfer coefficients at low and high wind speeds. In this paper, we also provide an accurate formulation of air–sea fluxes using stability-dependent exchange coefficients, allowing the use of ocean model sea surface temperature (SST) in their calculation for a wide range of atmospheric conditions over the global ocean. This approach can substantially improve the accuracy of an ocean model simulated–SSTs by providing a physically natural tendency toward accurate SSTs without relaxation to any SST data or climatology.

The main purposes of this study are to present (i) exchange coefficients based on the COARE v3.0 (section 2) and (ii) polynomial parameterizations of C_D, C_L, and C_S based on these coefficients (section 3). In particular, the stability correction in these parameterizations is approximated by a term depending on the $(T_a - T_s)$ and a polynomial function of the V_a at 10 m using tabulated exchange coefficients as obtained from the COARE algorithm (v3.0). A virtual temperature-based correction to $(T_a - T_s)$ is later applied to the polynomial functions, thus including the effects of water vapor flux on the exchange coefficients (section 4). Finally, exchange coefficients presented in sections 3 and 4 are used for calculating climatological mean wind stress magnitude in the North Pacific Ocean over 1979–93 (section 5).

2. The COARE exchange coefficients

The COARE algorithm (v3.0) presented in Fairall et al. (2003) is based on previously published results and 2777 one-hour covariance flux measurements. Fairall et al. (2003) added 4439 new values from field experiments between 1997 and 1999 to test the algorithm. The new observational dataset now dominates the database, especially in the wind speed regime above 10 m s^{-1}, where the number of observations increased from 67 to about 800. After applying quality controls, the database was used to evaluate the algorithm. The average (mean and median) model results agreed with the measurements to within about 5% for moisture from 0 to 20 m s^{-1}. For stress, the covariance measurements were about 10% higher than the model at wind speeds over 15 m s^{-1} while inertial-dissipation measurements agreed closely at all wind speeds. Thus, it should be emphasized that the COARE algorithm (v3.0) is considered to be the state-of-the-art algorithm in this paper.

For the purpose of this paper, the COARE algorithm (v3.0) was modified to produce C_D and C_L at various $(T_a - T_s)$ and V_a intervals over the global ocean. In

particular, the algorithm was run using various values of T_s, relative humidity (RH) just above the sea surface, T_a, and V_a. There is no cool skin or warm-layer calculation; thus, a skin sea surface temperature value is used in the algorithm. The use of a bulk value is an approximation, which allows one to perform the calculation without specifying radiative parameters or a time history of the fluxes. The roughness length for temperature is assumed equal to that for humidity in the algorithm; thus, C_L is equal to C_S in this paper.

In addition to $(T_a - T_s)$ and V_a, the effect of any water vapor flux through RH must be taken into account in calculating the exchange coefficients at low winds, a topic which will be discussed in section 4 in detail. In this section the exchange coefficients are obtained for a relatively low T_s (10°C) and for humidity close to or at saturation (RH = 100%) to investigate the impact of only $(T_a - T_s)$ on C_D and C_L. Note that dividing the mixing ratio (q_a) by the saturation mixing ratio (q_{sat}) and then multiplying this number by 100 determines the RH (in %). A T_s value of 10°C was chosen for consistency with the COARE algorithm testing, and because almost no sensitivity to the choice of T_s was found. This is true since the only effect of the temperature in the COARE algorithm enters through the nonlinearity of the saturation vapor pressure for water vapor, which has some effect at 30°C and upward.

Exchange coefficients for C_D and C_L are first generated using an RH value of 100% for various $(T_a - T_s)$ ranging from −8° to 7°C: 7°, 6°, 5°, 4°, 3°, 2°, 1°, 0.75°, 0.5°, 0.25°, 0, −0.098°, −0.25°, −0.75°, −1°, −2°, −3°, −4°, −6°, −8°C. These values were chosen to represent a wide variety of $(T_a - T_s)$ intervals over the global ocean. It is noted that a $(T_a - T_s)$ value of ≈−0.098° gives the neutral stability value. The resolution of $(T_a - T_s)$ intervals was increased near the neutral stability value to better examine behavior of exchange coefficients with respect to stability. In addition, the 10-m wind speed values of 1–40 m s^{-1} with increments of 1 m s^{-1} were used to determine coefficients at both low and high wind speed conditions (e.g., tropical cyclones and hurricanes).

Figure 1 shows C_D and C_L values obtained from the COARE algorithm when RH is set to 100%. Both C_D and C_L experience large changes with wind speed at 10 m above sea surface, and they are also quite different with respect to $(T_a - T_s)$ values for a given wind speed. In general, C_D is always greater than 2.0×10^{-3} at $V_a > 20$ m s^{-1} for any given $(T_a - T_s)$ value (Fig. 1a). On the other hand, C_L does not have any significant variability at high wind speeds (Fig. 1b). In particular, C_L is almost constant with values ranging between $\approx 1.2 \times 10^{-3}$ and $\approx 1.3 \times 10^{-3}$ for any given $(T_a - T_s)$ values above 20 m s^{-1}. There are strong variations in the exchange coefficients with respect to $(T_a - T_s)$ at very low wind speeds ($V_a < 3$ m s^{-1}), and this is especially evident at V_a values of 1 and 2 m s^{-1} (Figs. 1c,d). The $V_a = 1$ m s^{-1} cases are intended to show how variable C_D and C_L can be at very low wind speed regimes. Even the C_D and C_L values for $V_a = 1$ m s^{-1} are quite different from those for $V_a = 2$ m s^{-1}. We actually obtained C_D and C_L values from the COARE algorithm at each 1 m s^{-1} interval up to 40 m s^{-1}, but they are only shown at 2 m s^{-1} intervals in the figure for visual clarity. Although exchange coefficients can exist for $V_a = 0$ m s^{-1}, they are ignored in the analyses because air–sea fluxes are quite small under calm wind conditions.

The impact of stability through $(T_a - T_s)$ on both C_D and C_L is clearly evident from Fig. 1. Thus, exchange coefficients reduced to neutral stability, based solely on wind speed at 10 m above the sea surface (e.g., Large and Pond 1981), with no stability dependence (that is, $T_a - T_s = 0$ and/or at saturated conditions), will not be appropriate when they are used in OGCM simulations. This becomes a critical issue in model simulations, especially when studying the diurnal cycle of upper ocean quantities.

Regarding hurricane-force winds (e.g., $V_a > 30$ m s^{-1}), there is almost no direct experimental evidence for determining exchange coefficients. There are very few direct observations of exchange coefficients for wind speeds greater than 25 m s^{-1}. As to C_L and C_S, there is the problem of spray (e.g., Andreas and Emanuel 2001; Emanuel 2003). The COARE algorithm used here includes an option to define roughness length in terms of the sea state. It includes a formula based on wave age (Oost et al. 2002) or one based on significant height and slope of the waves (Taylor and Yelland 2001). The latter formula predicts significantly lower roughness at high wind speeds compared to the former one as explained by Taylor and Yelland (2003) who evaluated performance of the different formulas in predicting the C_D. Based on evidence from laboratory studies (e.g., Keller et al. 1992) and comparisons with field experiments (e.g., Janssen 1997; Johnson et al. 1998), the formula proposed by Taylor and Yelland (2001), as used in the COARE algorithm, is applicable over most conditions. It also succeeds at high winds and very short fetches in wind-wave flumes when wave age formulas fail.

It should be emphasized that there is very little reason for the exchange coefficients obtained from the algorithm to change geographically. The main change from one area to another would be due to different stability or different temperature levels, but any such

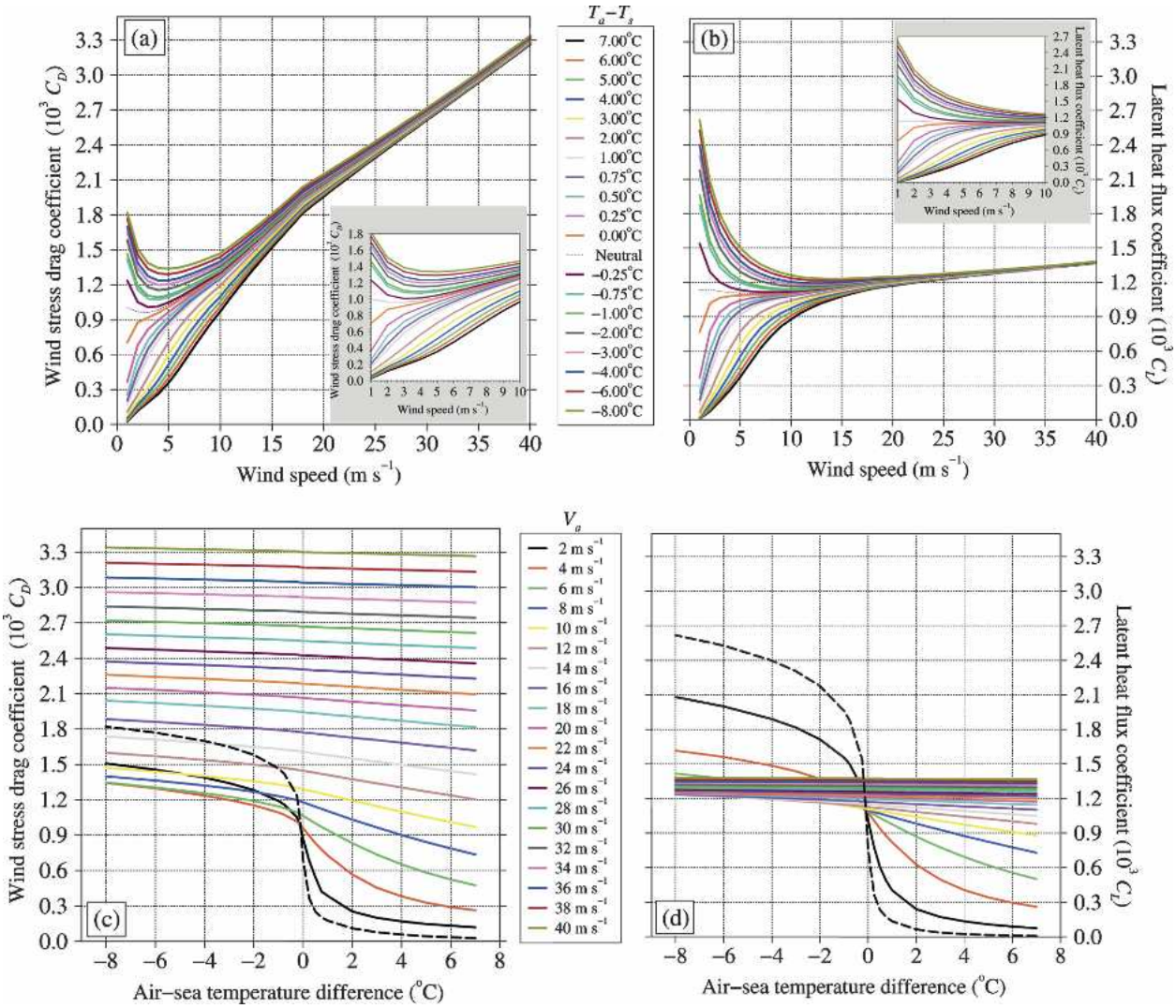

FIG. 1. Variations of exchange coefficients with respect to ($T_a - T_s$) and V_a values obtained from the COARE (v3.0) algorithm: (a) C_D values plotted against the observed 10 m V_a; (b) C_L values plotted against the observed 10 m V_a; (c) C_D values plotted against the observed ($T_a - T_s$), where T_a is at 10 m; and (d) C_L values plotted against the observed ($T_a - T_s$), where T_a is at 10 m. The small panels inside (a) and (b) are intended to show variability of C_D and C_L for only $V_a \leq 10$ m s^{-1}, respectively. Dashed lines in (c) and (d) show C_D and C_L values for $V_a = 1$ m s^{-1}. It is noted that the bulk formulas are $Q_L = C_L\, L\, \rho_a\, V_a\, (q_a - q_s)$ for latent heat flux, $Q_s = C_S\, C_p\, \rho_a\, V_a\, (T_a - T_s)$ for sensible heat flux, and $\tau = \rho_a C_D V_a^2$ for wind stress. Here, L is the latent heat of vaporization (2.5×10^6 J kg^{-1}), $\rho_a = 100\, P_a/[R_{\text{gas}}\, (T_a + 273.16)]$ (in kg m^{-3}), where R_{gas} is the gas constant (287.1 J kg^{-1} K^{-1}), and P_a is the mean sea level pressure.

changes should be dealt with by the algorithm. The only other possible changes are 1) the change in gravity, which increases by up to 0.5% going from equator to the Pole; and 2) the nominal atmospheric boundary layer depth (600 m) used, which is also realistic in most areas. Another possible effect with geographic variation is the sea state. While the effect of sea state on surface roughness is debatable, it is usually negligible, say for $V_a > 10$ m s^{-1} and in deep water, as mentioned in Taylor and Yelland (2001).

3. Polynomial approach for exchange coefficients

The exchange coefficients (C_D and C_L) are dependent on both V_a and ($T_a - T_s$) as discussed in section 2 (see Fig. 1). The effect of RH on C_D and C_L will be added to the polynomial functions as a correction term because including the full stability conditions (i.e., both $T_a - T_s$ and RH) in polynomial equations is not straightforward (see section 4).

We first investigate whether or not C_D and C_L can

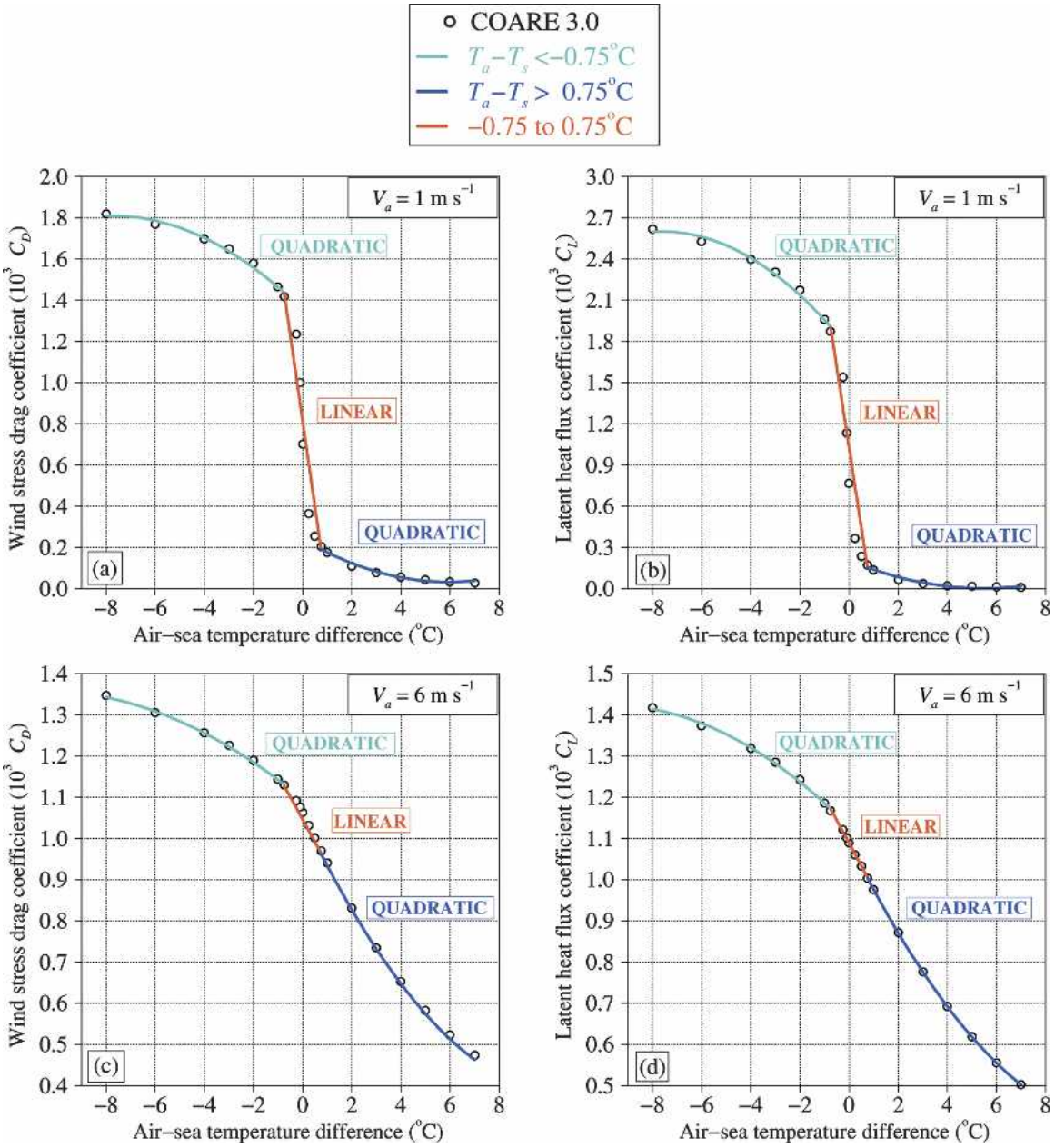

FIG. 2. Examples of applying optimal polynomial fits to the exchange coefficients: (a) C_D for $V_a = 1$ m s^{-1}, (b) C_L for $V_a = 1$ m s^{-1}, (c) C_D for $V_a = 6$ m s^{-1}, and (d) C_L for $V_a = 6$ m s^{-1}. Note that the exchange coefficients shown with open circles are obtained from the COARE algorithm.

be expressed as simple polynomial functions of V_a and $(T_a - T_s)$ using C_D and C_L values when humidity is close to or at saturation (i.e., RH = 100%). For this purpose, C_D and C_L values are plotted against $(T_a - T_s)$ for each V_a value. As an example, Fig. 2 shows variation of exchange coefficients with respect to $(T_a - T_s)$ for $V_a = 1$ m s^{-1} and $V_a = 6$ m s^{-1}, suggesting that we can construct polynomial functions in $(T_a - T_s)$ with coefficients that vary with V_a. We split the whole $(T_a - T_s)$ range (from −8.00° to 7.00°C) into three subranges. The reason for this split was that there was no simple (low order) polynomial fit for C_D and C_L at low wind speeds when using the whole $(T_a - T_s)$ range.

Various $(T_a - T_s)$ intervals were tested to obtain the best available lowest-order polynomial function for the exchange coefficients. After a few tests, we found three ranges for $(T_a - T_s)$: 1) $-8.00°\text{C} \le T_a - T_s < -0.75°\text{C}$, 2) $-0.75°\text{C} \le T_a - T_s \le 0.75°\text{C}$, and 3) $0.75°\text{C} < T_a - T_s \le 7.00°\text{C}$. Hereinafter, for convenience, these inter-

vals will be referred to as unstable, neutral, and stable cases, respectively. As evident from Fig. 2, it was possible to represent the neutral case using a linear equation, and the other two ranges (stable and unstable cases) by a quadratic equation for C_D and C_L. Obviously, a higher polynomial fit would fit better for the neutral case (e.g., Figs. 2a,b) but the use of the linear function is preferred for computational efficiency. The resulting error with respect to the COARE algorithm would also be negligible because a wind speed of 1 m s^{-1} entering the bulk formulations of wind stress and latent heat flux is also small for these two distinct cases.

We obtained a single equation for C_D and C_L that represents all wind speeds from V_a values of 1–40 m s^{-1}. Given that a quadratic polynomial is suitable for unstable and stable cases, and a linear fit is suitable for the neutral case, we then write a generalized polynomial equation for C_D as follows:

$$C_D = \begin{cases} C_{D0}(V_a) + C_{D1}(V_a)(T_a - T_s) + C_{D2}(V_a)(T_a - T_s)^2 & \text{for} \quad -8.00^\circ\text{C} \le T_a - T_s < -0.75^\circ\text{C}, \\ C_{D0}(V_a) + C_{D1}(V_a)(T_a - T_s) & \text{for} \quad -0.75^\circ\text{C} \le T_a - T_s \le 0.75^\circ\text{C}, \\ C_{D0}(V_a) + C_{D1}(V_a)(T_a - T_s) + C_{D2}(V_a)(T_a - T_s)^2 & \text{for} \quad 0.75^\circ\text{C} < T_a - T_s \le 7.00^\circ\text{C}. \end{cases} \tag{1}$$

The same type of equations are also written for C_L as follows:

$$C_L = \begin{cases} C_{L0}(V_a) + C_{L1}(V_a)(T_a - T_s) + C_{L2}(V_a)(T_a - T_s)^2 & \text{for} \quad -8.00^\circ\text{C} \le T_a - T_s < -0.75^\circ\text{C}, \\ C_{L0}(V_a) + C_{L1}(V_a)(T_a - T_s) & \text{for} \quad -0.75^\circ\text{C} \le T_a - T_s \le 0.75^\circ\text{C}, \\ C_{L0}(V_a) + C_{L1}(V_a)(T_a - T_s) + C_{L2}(V_a)(T_a - T_s)^2 & \text{for} \quad 0.75^\circ\text{C} < T_a - T_s \le 7.00^\circ\text{C}. \end{cases} \tag{2}$$

Unlike Kara et al. (2000, 2002), there are no limits set on V_a in these formulations because we were able to take low and high wind speed values into account in the algorithms by using V_a of 1, 2, and 3 m s^{-1} as obtained from the COARE algorithm.

The next step is to obtain C_{D0}, C_{D1}, and C_{D2} values (and similarly C_{L0}, C_{L1}, and C_{L2} values) to be used in the generalized equations of (1) and (2). To accomplish this, the example of the curve-fitting process shown in Fig. 2 for V_a values of 1 and 6 m s^{-1} is repeated for each V_a value ranging from 1 to 40 m s^{-1} (with 1 m s^{-1} increments). Thus, for example, the quadratic fits to C_D for the unstable case yielded a total of 40 C_{D0}, 40 C_{D1}, and 40 C_{D2} values. Applying a linear fit would be sufficient for unstable and stable cases when $V_a \ge 10$ m s^{-1}, but for consistency a quadratic fit was used for all V_a values.

The final step is to express C_{D0}, C_{D1}, and C_{D2} values (similarly for C_{L0}, C_{L1}, and C_{L2} values) as polynomial functions of V_a or V_a^{-1}, representing all V_a values from 1 to 40 m s^{-1}. However, there was no single low-order polynomial equation for the whole V_a range using all 40 of the C_{D0}, C_{D1}, and C_{D2} values. This is not suprising because both C_D and C_L vary significantly at low wind speeds as shown before (see Figs. 1c,d). Therefore, we used two V_a intervals: 1) $V_a \le 5$ m s^{-1} and 2) $V_a \ge 5$ m s^{-1}. Figure 3 shows C_{D0} and C_{L0} values for the $V_a \le 5$ m s^{-1} case. While a cubic fit worked best for C_{D0}, a quadratic fit is sufficient for C_{L0}. In the unstable case, we can then write $C_{D0} = 1.89100 - 0.71820\ V_a + 0.19750\ V_a^2 - 0.01790\ V_a^3$ and $C_{L0} = 2.07700 - 0.39330\ V_a + 0.03971\ V_a^2$.

Polynomial coefficients for C_D and C_L are given in Table 1 for unstable, neutral, and stable cases. Note that the best fit is sometimes obtained when using V_a^{-1} rather than V_a as the dependent variable. Since V_a^{-1} is being used in some cases, there must be a minimum for V_a. Here the minimum V_a considered is 1 m s^{-1}. It is also important to note that we obtained all polynomial functions such that they match up at $V_a = 5$ m s^{-1}, and at $(T_a - T_s)$ values of -0.75° and 0.75°C, as well.

4. Relative humidity effects on exchange coefficients

The polynomial functions presented in section 3 were determined using exchange coefficients from the COARE v3.0 algorithm, which was run for various $(T_a - T_s)$ values at RH = 100%, ignoring the impact of RH on the exchange coefficients. This simply implies that in our approximations so far, by far the major effect of water vapor on C_D and C_L is its temperature-dependent impact on stability, which is very large in the Tropics and decreases with decreasing absolute temperature. Because of the exponential increase of saturation vapor pressure with temperature, in regions such as the Tropics, humidity has a first-order effect on the stability, and since the Tropics tend to be light wind areas, on the fluxes as well.

Here, our purpose is to include full atmospheric sta-

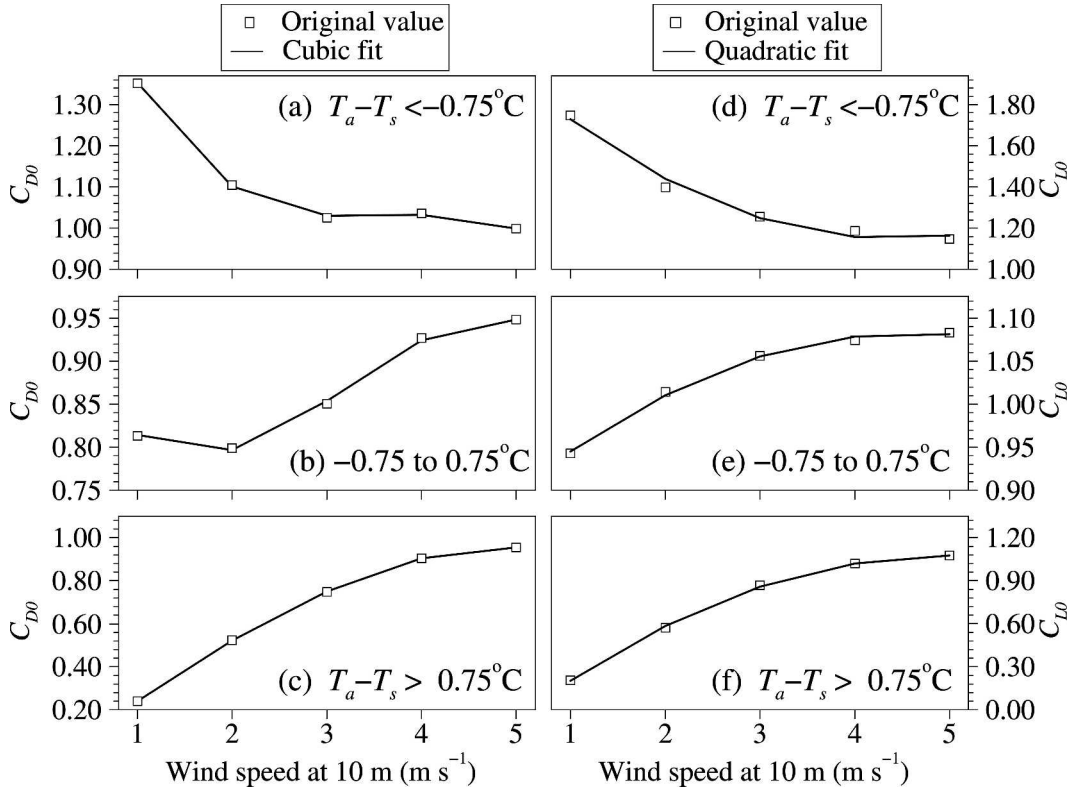

FIG. 3. The wind speed dependence values of C_{D0} and C_{L0}. Results are shown for $V_a \leq 5$ m s^{-1} cases for each given $(T_a - T_s)$ interval.

bility in the polynomial functions (see section 3) by using water vapor in addition to $(T_a - T_s)$ and V_a. The exchange coefficients calculated using these full stability conditions will be correct over a wide range of conditions. For example, our polynomial approach is applicable to conditions where the water vapor (including RH) makes a significant contribution to the buoyancy flux, that is, when the full impact of stability on the air–sea fluxes is included. Similarly, one would not expect any significant error when T_a is warmer than T_s, but the water vapor results in unstable stratification.

The polynomial functions for C_D and C_L shown in section 3 assume saturated conditions (i.e., RH = 100%). However, water vapor effects can be taken into account via a virtual temperature-based correction to $(T_a - T_s)$. The virtual air temperature (T_{va}) is calculated from the mixing ratio at 10 m above the sea surface (q_a) using $T_{va} = T_a\,[1 + 0.61\,q_a(T_a)]$ with T_a in Kelvins (K). One possible approach would be recast the polynomial functions for C_D and C_L to be functions of $(T_{va} - T_{vs})$ rather than $(T_a - T_s)$. Since we already have polynomial functions for saturated conditions, we instead apply a correction that is zero when RH = 100%:

$$(T_a - T_s)_c = (T_a - T_s) - 0.61\,T_a(q_{\rm sat} - q_a), \quad (3)$$

where $q_{\rm sat}$ is the saturation mixing ratio at T_a from a simplified version of the original formulation for saturated vapor-pressure presented by Lowe (1977), which has a computational advantage over Buck (1981).

The polynomial functions for C_D and C_L applied to $(T_a - T_s)_c$ are obviously identical to the original approach or saturated conditions and are in good agreement with the COARE algorithm (v3.0) for all relative humidities (not shown). Once the correction is applied to the polynomial functions, exchange coefficients are calculated. It is emphasized that in the polynomial functions one could use very fine increments for $(T_a - T_s)$ rather than those used in the original COARE algorithm (see section 2) to calculate C_D and C_L because all polynomials are continuous for any given $(T_a - T_s)$, V_a, and RH.

Using the tabulated exchange coefficients obtained from the polynomial functions, we now investigate the impact of RH (0%–100%) in calculating C_D and C_L. It is clear that assuming an RH value of 100% results in significant errors for $V_a = 1$ m s^{-1} (Fig. 4). The impact of RH on C_D and C_L is clearly seen when the difference between T_a and T_s is small (e.g., $-2°\text{C} \leq \text{T}_a - T_s < 2°\text{C}$). Such a result clearly demonstrates that atmospheric stability can be predicted incorrectly when ig-

TABLE 1. Optimal polynomial coefficients for C_D and C_L. They are shown for $V_a \leq 5$ m s^{-1} and $V_a \geq 5$ m s^{-1} separately. Note that C_D and C_L coefficients are continuous at $V_a = 5$ m s^{-1}, $(T_a - T_s) = -0.75$°C, and $(T_a - T_s) = 0.75$°C.

Wind speed		Cubic	Polynomial coefficients 0	1	2	3
				$-8.00° \text{ C} \leq T_a - T_s < -0.75$°C		
$V_a \leq 5$ m s^{-1}	C_{D0}	V_a	1.891 00	−0.718 20	0.197 50	−0.017 90
	C_{D1}	V_a^{-1}	−0.006 30	−0.302 80	0.312 00	−0.121 00
	C_{D2}	V_a^{-1}	0.000 44	−0.017 69	0.013 03	−0.003 39
$V_a \geq 5$ m s^{-1}	C_{D0}	V_a	0.649 70	0.069 93	3.54e-5	−3.43e-6
	C_{D1}	V_a^{-1}	0.003 83	−0.275 60	−1.091 00	4.946 00
	C_{D2}	V_a^{-1}	−4.83e-5	0.007 71	−0.255 50	0.765 40
				$-0.75°\text{C} \leq T_a - T_s \leq 0.75°$C		
$V_a \leq 5$ m s^{-1}	C_{D0}	V_a	0.977 40	−0.256 60	0.104 80	−0.010 97
	C_{D1}	V_a^{-1}	0.205 10	−1.903 00	1.133 00	−0.265 80
$V_a \geq 5$ m s^{-1}	C_{D0}	V_a	0.543 80	0.083 16	−0.000 49	3.09e-6
	C_{D1}	V_a^{-1}	−0.016 69	0.573 80	−12.240 00	32.530 00
				$0.75°\text{C} < T_a - T_s \leq 7.00°$C		
$V_a \leq 5$ m s^{-1}	C_{D0}	V_a	−0.066 95	0.313 30	−0.001 47	−0.004 06
	C_{D1}	V_a^{-1}	0.099 66	−2.116 00	4.626 00	−2.680 00
	C_{D2}	V_a^{-1}	−0.024 77	0.272 60	−0.555 80	0.313 90
$V_a \geq 5$ m s^{-1}	C_{D0}	V_a	0.558 10	0.081 74	−0.000 45	2.67e-6
	C_{D1}	V_a^{-1}	−0.005 59	0.209 60	−8.634 00	18.630 00
	C_{D2}	V_a^{-1}	0.000 60	−0.026 29	0.212 10	0.775 50
		Quadr.		$-8.00°\text{C} \leq T_a - T_s \leq -0.75°$C		
$V_a \leq 5$ m s^{-1}	C_{L0}	V_a	2.077 00	−0.393 30	0.039 71	·
	C_{L1}	V_a	−0.289 90	0.073 50	−0.006 27	·
	C_{L2}	V_a	−0.019 54	0.005 48	−0.000 49	·
$V_a \geq 5$ m s^{-1}	C_{L0}	V_a	1.074 00	0.005 58	5.26e-5	·
	C_{L1}	V_a^{-1}	0.006 91	−0.224 40	−1.027 00	·
	C_{L2}	V_a^{-1}	0.000 19	−0.002 18	−0.101 00	·
				$-0.75°\text{C} \leq T_a - T_s < 0.75°$C		
$V_a \leq 5$ m s^{-1}	C_{L0}	V_a	0.858 00	0.097 43	−0.010 56	·
	C_{L1}	V_a	−1.927 00	0.734 50	−0.077 06	·
$V_a \geq 5$ m s^{-1}	C_{L0}	V_a	1.023 00	0.009 61	−2.16e-5	·
	C_{L1}	V_a^{-1}	−0.003 93	0.204 80	−5.048 00	·
				$0.75°\text{C} < T_a - T_s \leq 7.00°$C		
$V_a \leq 5$ m s^{-1}	C_{L0}	V_a	−0.29250	0.549 80	−0.055 44	·
	C_{L1}	V_a	0.073 72	−0.174 00	0.024 89	·
	C_{L2}	V_a	−0.006 95	0.016 37	−0.002 62	·
$V_a \geq 5$ m s^{-1}	C_{L0}	V_a	1.023 00	0.00966	−2.28e-5	·
	C_{L1}	V_a^{-1}	−0.00267	0.210 30	−5.329 00	·
	C_{L2}	V_a^{-1}	0.001 55	−0.062 28	0.509 40	·

noring RH dependence (i.e., assuming humidity close to or at saturation) in calculating C_D and C_L at low wind speeds. Overall, the direct effect of decreasing RH is to generally increase exchange coefficients as seen from the scatterplots of C_D and C_L for $V_a = 1$ m s^{-1} (Fig. 5). For example, if RH were 20% and one assumed an RH value of 100%, then C_D would be underestimated with ≈6 times less than its actual value (0.176×10^{-3} instead of 0.762×10^{-3}) for $V_a = 1$ m s^{-1} and $T_a - T_s = 1.0$°C (Table 2). Similarly, the underestimate of C_L would be ≈7 times less than its actual value (0.220×10^{-3} instead of 1.626×10^{-3}) for $V_a = 1$ m s^{-1} and $T_a - T_s = 0.7$°C (Table 2). On the other hand, it must be noted that the effect of RH on exchange coefficients is relatively small for high wind speeds as can be seen in C_D and C_L values for $V_a = 6$ m s^{-1} (Table 3). While the water vapor effect is most important at low wind speed, the reader is cautioned that low wind speed implies small wind stress and small latent and sensible heat fluxes. If the wind stress or latent and sensible heat flux values are small to start with, even an extremely large change in their strength might still mean small values after the RH effect is taken into account. For example, latent heat flux at $V_a = 1$ m s^{-1} is ≈1.9 W m^{-2} (≈11.8 W m^{-2}) when RH = 100% (RH = 20%). In both estimates we use $T_a - T_s = 2$°C, and $q_a - q_s = 3$ g kg^{-1}.

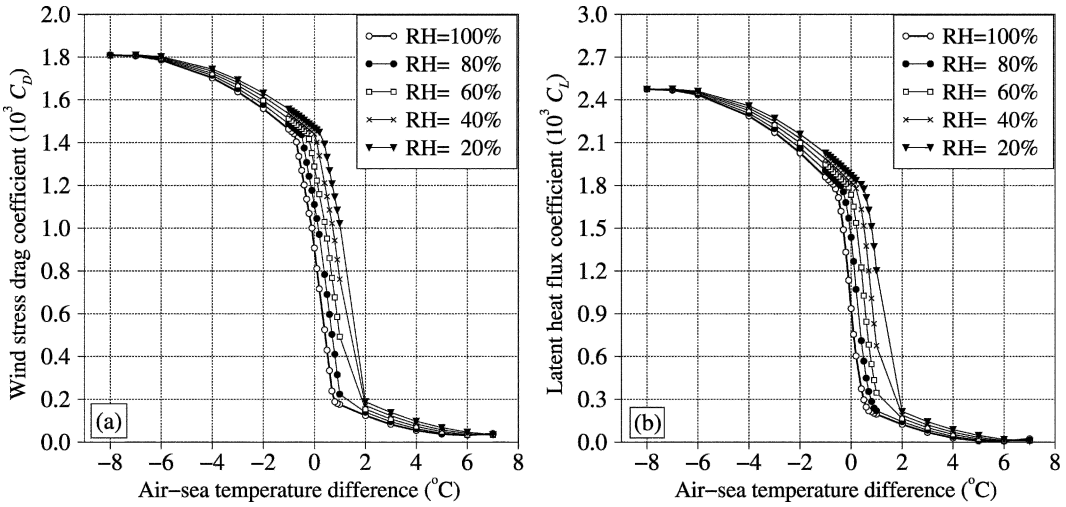

FIG. 4. Exchange coefficients plotted against various ($T_a - T_s$) values at $V_a = 1$ m s^{-1} as determined from the polynomial functions: (a) C_D and (b) C_L. This figure demonstrates variability of exchange coefficients with water vapor. Results are shown for RH values of 20%, 40%, 60%, 80%, and 100%.

5. Wind stress magnitude over the North Pacific Ocean

As an example, results from calculating wind stress magnitude based on the stability dependent C_D is demonstrated in the North Pacific Ocean (Fig. 6). All analyses are based on 6-hourly meteorological data from an archived product, the 40-yr European Centre for Medium-Range Weather Forecasts (ECMWF) Re-Analysis (ERA-40; Simmons and Gibson 2000). A climatological mean wind stress magnitude is formed over 1979–93. This time period was chosen to be consistent with ERA-15, which has been extensively used in previous ocean modeling studies (e.g., Hurlburt and Hogan 2000; Kara et al. 2004). In addition, all fields shown are interpolated onto the 1/12° Hybrid Coordinate Ocean Model (HYCOM) domain to demonstrate possible problems when using atmospheric variables (e.g., wind stress fields) from coarse-resolution archived products (e.g., 1.125°ERA-40 data) in forcing much finer OGCMs (e.g., 1/12° HYCOM). Basic features and a description of HYCOM are given in Kara et al. (2005).

We first form a climatological mean total wind stress magnitude field (Fig. 6a) using zonal and meridional

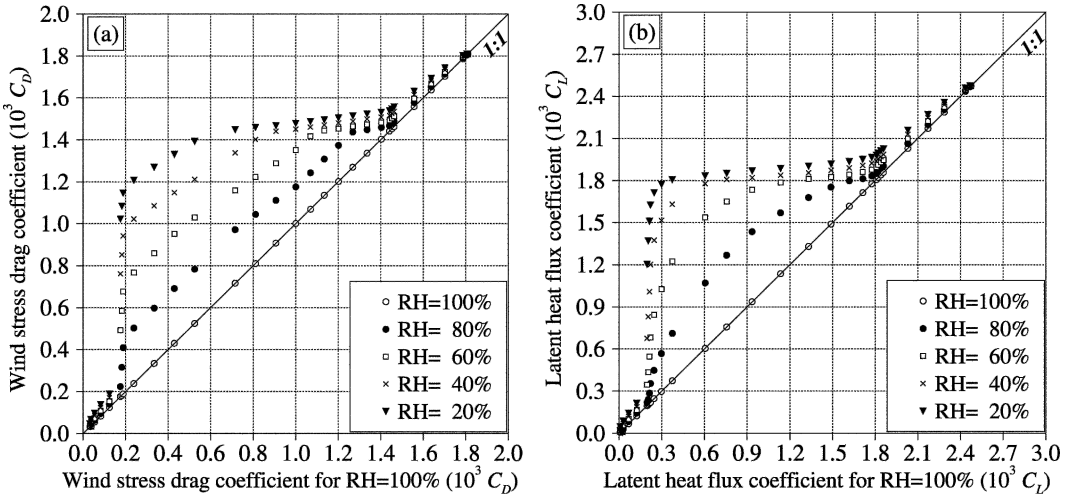

FIG. 5. Scatterplots of exchange coefficients for RH = 100% vs those for varying RH values at $V_a = 1$ m s^{-1} (see also Fig. 4): (a) C_D and (b) C_L. The diagonal line identifies almost universal increase in exchange coefficients for given RH values against those for RH = 100%.

TABLE 2. Exchange coefficients for varying RH values and ($T_a - T_s$) intervals at $V_a = 1$ m s^{-1} as determined from the polynomial functions. Also given are C_D (RH)/C_D (RH = 100%) ratios. In the table, for example, C_D (80%)/C_D (RH = 100%) is the ratio of C_D for RH = 80% to that for RH = 100%. Note that all exchange coefficients must be multiplied by 10^{-3}.

$T_a - T_s$	C_D for varying RH at $V_a = 1$ m s^{-1}						C_D (RH)/C_D (RH = 100%)					
(°C)	100%	80%	60%	40%	20%	00%	100%	80%	60%	40%	20%	0%
7.000	0.039	0.035	0.033	0.032	0.035	0.039	1.00	0.90	0.85	0.82	0.90	1.00
6.000	0.032	0.033	0.035	0.040	0.046	0.054	1.00	1.03	1.09	1.25	1.44	1.69
5.000	0.037	0.042	0.049	0.057	0.067	0.079	1.00	1.14	1.32	1.54	1.81	2.14
4.000	0.054	0.063	0.073	0.085	0.098	0.112	1.00	1.17	1.35	1.57	1.81	2.07
3.000	0.083	0.095	0.108	0.123	0.138	0.155	1.00	1.14	1.30	1.48	1.66	1.87
2.000	0.124	0.139	0.154	0.171	0.189	0.445	1.00	1.12	1.24	1.38	1.52	3.59
1.000	0.176	0.223	0.493	0.762	1.023	1.212	1.00	1.27	2.80	4.33	5.81	6.89
0.700	0.239	0.503	0.767	1.022	1.208	1.393	1.00	2.10	3.21	4.28	5.05	5.83
0.500	0.430	0.690	0.951	1.148	1.331	1.449	1.00	1.60	2.21	2.67	3.10	3.37
0.200	0.716	0.971	1.159	1.338	1.449	1.477	1.00	1.36	1.62	1.87	2.02	2.06
0.000	0.907	1.111	1.288	1.441	1.468	1.495	1.00	1.22	1.42	1.59	1.62	1.65
−0.098	1.000	1.176	1.351	1.451	1.478	1.504	1.00	1.18	1.35	1.45	1.48	1.50
−0.200	1.069	1.243	1.417	1.461	1.487	1.512	1.00	1.16	1.32	1.37	1.39	1.41
−0.700	1.403	1.458	1.483	1.508	1.532	1.554	1.00	1.03	1.06	1.07	1.09	1.11
−1.000	1.463	1.488	1.512	1.535	1.557	1.578	1.00	1.02	1.03	1.05	1.06	1.08
−2.000	1.558	1.578	1.597	1.615	1.632	1.648	1.00	1.01	1.03	1.04	1.05	1.06
−3.000	1.638	1.653	1.668	1.681	1.694	1.707	1.00	1.01	1.02	1.03	1.03	1.04
−4.000	1.703	1.714	1.724	1.734	1.744	1.752	1.00	1.01	1.01	1.02	1.02	1.03
−6.000	1.787	1.791	1.795	1.799	1.802	1.804	1.00	1.00	1.00	1.01	1.01	1.01
−8.000	1.810	1.809	1.808	1.807	1.805	1.803	1.00	1.00	1.00	1.00	1.00	1.00
$T_a - T_s$	C_L for varying RH at $V_a = 1$ m s^{-1}						C_L (RH)/C_L (RH = 100%)					
(°C)	100%	80%	60%	40%	20%	0%	100%	80%	60%	40%	20%	0%
7.000	0.023	0.014	0.009	0.006	0.007	0.011	1.00	0.61	0.39	0.26	0.30	0.48
6.000	0.007	0.006	0.008	0.012	0.019	0.029	1.00	0.86	1.14	1.71	2.71	4.14
5.000	0.009	0.015	0.023	0.033	0.046	0.061	1.00	1.67	2.56	3.67	5.11	6.78
4.000	0.029	0.040	0.054	0.069	0.087	0.107	1.00	1.38	1.87	2.38	3.00	3.69
3.000	0.067	0.083	0.101	0.121	0.143	0.166	1.00	1.24	1.51	1.81	2.13	2.48
2.000	0.123	0.143	0.165	0.189	0.214	0.308	1.00	1.16	1.34	1.54	1.74	2.50
1.000	0.196	0.219	0.345	0.675	1.203	1.633	1.00	1.12	1.76	3.44	6.14	8.33
0.700	0.220	0.354	0.683	1.202	1.626	1.806	1.00	1.61	3.10	5.46	7.39	8.21
0.500	0.297	0.567	1.027	1.517	1.773	1.834	1.00	1.91	3.46	5.11	5.97	6.18
0.200	0.604	1.071	1.538	1.778	1.835	1.884	1.00	1.77	2.55	2.94	3.04	3.12
0.000	0.936	1.436	1.734	1.820	1.869	1.916	1.00	1.53	1.85	1.94	2.00	2.05
−0.098	1.136	1.570	1.786	1.838	1.886	1.932	1.00	1.38	1.57	1.62	1.66	1.70
−0.200	1.331	1.679	1.811	1.856	1.902	1.948	1.00	1.26	1.36	1.39	1.43	1.46
−0.700	1.809	1.850	1.896	1.940	1.982	2.022	1.00	1.02	1.05	1.07	1.10	1.12
−1.000	1.859	1.904	1.946	1.987	2.026	2.064	1.00	1.02	1.05	1.07	1.09	1.11
−2.000	2.029	2.064	2.098	2.130	2.160	2.190	1.00	1.02	1.03	1.05	1.06	1.08
−3.000	2.171	2.198	2.224	2.248	2.271	2.293	1.00	1.01	1.02	1.04	1.05	1.06
−4.000	2.287	2.306	2.325	2.342	2.358	2.374	1.00	1.01	1.02	1.02	1.03	1.04
−6.000	2.435	2.442	2.449	2.455	2.460	2.465	1.00	1.00	1.01	1.01	1.01	1.01
−8.000	2.474	2.474	2.474	2.474	2.474	2.474	1.00	1.00	1.00	1.00	1.00	1.00

wind stress components that are directly output at 6-hourly time intervals from ERA-40. This field is obtained from the planetary boundary layer model in the ECMWF atmospheric model. There is excessive noise in the wind stress magnitude near the coastal boundaries, such as along the eastern Pacific and in the Sea of Japan. This noise is a major motivation for recalculating the wind stress magnitude rather than using the one output from ERA-40. Thus, our purpose is to eliminate the noise shown in Fig. 6a, so that this field can be suitable as an atmospheric forcing field for an OGCM simulation. We recompute the wind stresses [$\boldsymbol{\tau} = (\tau_x, \tau_y)$] with a bulk formulation using C_D values as derived in sections 3 and 4 as follows:

$$\tau_x = \rho_a C_D u(u^2 + v^2)^{1/2}, \quad (4)$$

$$\tau_y = \rho_a C_D v(u^2 + v^2)^{1/2}, \quad (5)$$

$$\tau = \rho_a C_D(u^2 + v^2), \quad (6)$$

TABLE 3. Exchange coefficients for varying RH values and ($T_a - T_s$) intervals at $V_a = 6$ m s^{-1} as determined from the polynomial functions. Also given are C_D (RH)/C_D (RH = 100%) ratios. In the table, for example, C_D (80%)/C_D (RH = 100%) is the ratio of C_D for RH = 80% to that for RH = 100%. Note that all exchange coefficients must be multiplied by 10^{-3}.

$T_a - T_s$	C_D for varying RH at $V_a = 6$ m s^{-1}						C_D (RH)/C_D (RH = 100%)					
(°C)	100%	80%	60%	40%	20%	0%	100%	80%	60%	40%	20%	0%
7.000	0.443	0.463	0.485	0.509	0.535	0.563	1.00	1.05	1.09	1.15	1.21	1.27
6.000	0.493	0.516	0.541	0.568	0.596	0.627	1.00	1.05	1.10	1.15	1.21	1.27
5.000	0.554	0.580	0.608	0.637	0.667	0.699	1.00	1.05	1.10	1.15	1.20	1.26
4.000	0.627	0.655	0.685	0.716	0.748	0.781	1.00	1.04	1.09	1.14	1.19	1.25
3.000	0.712	0.742	0.773	0.805	0.838	0.873	1.00	1.04	1.09	1.13	1.18	1.23
2.000	0.807	0.839	0.871	0.904	0.939	0.991	1.00	1.04	1.08	1.12	1.16	1.23
1.000	0.915	0.949	1.000	1.051	1.096	1.100	1.00	1.04	1.09	1.15	1.20	1.20
0.700	0.952	1.002	1.052	1.096	1.100	1.105	1.00	1.05	1.11	1.15	1.16	1.16
0.500	0.988	1.037	1.086	1.099	1.103	1.111	1.00	1.05	1.10	1.11	1.12	1.12
0.200	1.042	1.090	1.099	1.103	1.111	1.123	1.00	1.05	1.05	1.06	1.07	1.08
0.000	1.078	1.098	1.102	1.108	1.119	1.131	1.00	1.02	1.02	1.03	1.04	1.05
−0.098	1.095	1.100	1.104	1.112	1.123	1.135	1.00	1.00	1.09	1.02	1.03	1.04
−0.200	1.097	1.101	1.105	1.116	1.128	1.139	1.00	1.00	1.01	1.02	1.03	1.04
−0.700	1.105	1.115	1.126	1.137	1.147	1.158	1.00	1.01	1.02	1.03	1.04	1.05
−1.000	1.117	1.128	1.139	1.149	1.159	1.169	1.00	1.01	1.02	1.03	1.04	1.05
−2.000	1.160	1.169	1.177	1.186	1.194	1.203	1.00	1.01	1.01	1.02	1.03	1.04
−3.000	1.198	1.205	1.212	1.219	1.226	1.233	1.00	1.00	1.01	1.02	1.02	1.03
−4.000	1.231	1.237	1.243	1.248	1.254	1.259	1.00	1.00	1.01	1.01	1.02	1.02
−6.000	1.283	1.287	1.291	1.294	1.297	1.300	1.00	1.00	1.00	1.01	1.01	1.01
−8.000	1.318	1.319	1.321	1.323	1.324	1.326	1.00	1.00	1.00	1.00	1.00	1.01

$T_a - T_s$	C_L for varying RH at $V_a = 6$ m s^{-1}						C_L (RH)/C_L (RH = 100%)					
(°C)	100%	80%	60%	40%	20%	0%	100%	80%	60%	40%	20%	00%
7.000	0.531	0.550	0.570	0.592	0.617	0.643	1.00	1.04	1.07	1.11	1.16	1.21
6.000	0.578	0.599	0.622	0.647	0.674	0.702	1.00	1.04	1.08	1.12	1.17	1.21
5.000	0.635	0.659	0.684	0.711	0.740	0.770	1.00	1.04	1.08	1.12	1.17	1.21
4.000	0.703	0.729	0.756	0.785	0.815	0.846	1.00	1.04	1.08	1.12	1.16	1.20
3.000	0.781	0.809	0.838	0.868	0.899	0.931	1.00	1.04	1.07	1.11	1.15	1.19
2.000	0.870	0.899	0.929	0.960	0.992	1.007	1.00	1.03	1.07	1.10	1.14	1.16
1.000	0.970	0.997	1.012	1.052	1.113	1.140	1.00	1.03	1.04	1.08	1.15	1.18
0.700	0.997	1.013	1.053	1.112	1.140	1.152	1.00	1.02	1.06	1.12	1.14	1.16
0.500	1.006	1.039	1.095	1.133	1.149	1.158	1.00	1.03	1.09	1.13	1.14	1.15
0.200	1.043	1.100	1.134	1.150	1.158	1.173	1.00	1.05	1.09	1.10	1.11	1.12
0.000	1.084	1.128	1.147	1.154	1.168	1.182	1.00	1.04	1.06	1.06	1.08	1.09
−0.098	1.108	1.136	1.150	1.159	1.173	1.187	1.00	1.03	1.04	1.05	1.06	1.07
−0.200	1.121	1.143	1.152	1.164	1.178	1.191	1.00	1.02	1.03	1.04	1.05	1.06
−0.700	1.152	1.163	1.176	1.189	1.201	1.213	1.00	1.01	1.02	1.03	1.04	1.05
−1.000	1.165	1.178	1.191	1.203	1.215	1.226	1.00	1.01	1.02	1.03	1.04	1.05
−2.000	1.215	1.226	1.236	1.246	1.256	1.265	1.00	1.01	1.02	1.03	1.03	1.04
−3.000	1.260	1.268	1.277	1.285	1.292	1.300	1.00	1.01	1.01	1.02	1.02	1.03
−4.000	1.298	1.305	1.311	1.318	1.324	1.330	1.00	1.01	1.01	1.02	1.02	1.02
−6.000	1.356	1.360	1.364	1.367	1.371	1.374	1.00	1.00	1.01	1.01	1.01	1.01
−8.000	1.391	1.391	1.391	1.391	1.391	1.391	1.00	1.00	1.00	1.00	1.00	1.00

where $V_a = (u^2 + v^2)^{1/2}$, $\tau = (\tau_x^2 + \tau_y^2)^{1/2}$, and u (v) is the zonal (meridional) wind speed component (m s^{-1}). Density of the air at the air–sea interface is obtained using $\rho_a = 100\ P_a/[R_{\text{gas}}\ (T_a + 273.16)]$ (in kg m^{-3}), where R_{gas} is the gas constant (287.1 J kg^{-1} K^{-1}) and P_a is the mean sea level pressure. All parameters needed for calculation of C_D, ρ_a, and wind stress magnitude (i.e., T_a, T_s, q_a, q_{sat}, u, v, P_a) are obtained from ERA-40 as mentioned earlier. Wind stress magnitude is computed at each 6-h interval and averaged over 1979–93.

The unrealistic noise along the coastlines is greatly cleaned up by using the bulk formulation with stability-dependent C_D based solely on $T_a - T_s$ (Fig. 6b). This is also true when calculating C_D depending on both $T_a - T_s$ and water vapor (Fig. 6c). The spatial patterns and approximate magnitude of the mean wind stress magnitude from the bulk formulation usually agree with

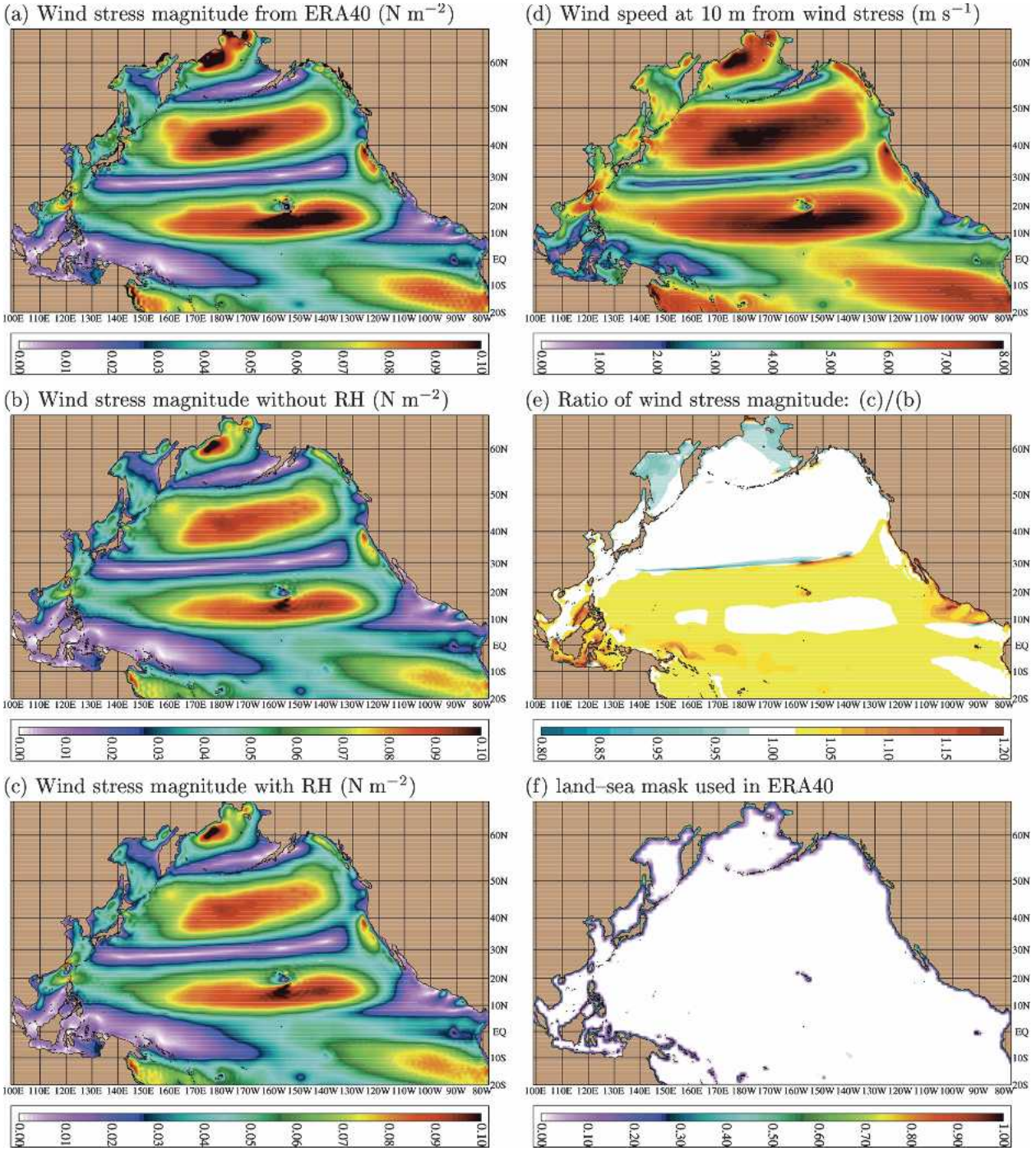

FIG. 6. Climatological mean wind stress magnitude over 1979–93 (a) as obtained directly from the ERA-40 output itself, (b) as computed from the bulk formulation using C_D ignoring RH effects (see section 3), and (c) as computed from the bulk formulation using C_D with the inclusion of RH effects (see section 4). Also shown are (d) wind speed at 10 m above the sea surface calculated from wind stress field shown in (c), (e) the ratio of wind stress magnitude calculated using (c)/(b), and (f) the land–sea mask from ERA-40, and note that a grid point is either land (1) or sea (0), giving values between 0 and 1 for interpolated the land–sea mask. All fields shown are interpolated on the 1/12° Mercator grid used in the Hybrid Coordinate Ocean Model (HYCOM).

those from ERA-40 itself. Basin-averaged mean wind stress magnitudes are 0.058, 0.034, and 0.037 N m^{-2} for Fig. 6a, Fig. 6b, and Fig. 6c, respectively. The relatively large basin-averaged mean value of 0.058 N m^{-2} in Fig. 6a is almost twice as large as those in Figs. 6b and 6c. This is due generally to the unrealistically large wind stress magnitudes near the land–sea boundaries, resulting from excessive noise in the original ERA-40 product.

The recomputed wind stress magnitude can also be used for determining V_a. Thus, excessive noise near the coastal boundaries can be removed from the V_a field as well (Fig. 6d). Here, assuming neutral C_D values, V_a is approximated using $V_a = 1/[\rho_a \times 10^{-3}\ (0.926 + 3.218\tau - 5.231\tau^2 + 3.236\tau^3)]$ for $\tau \leq 0.7711$ and $V_a = 1/[\rho_a \times 10^{-3}\ (1.461 + 0.485\tau - 0.092\tau^2 + 0.007\tau^3)]$ for $\tau > 0.7711$. The use of the wind stress magnitude field in Fig. 6c instead of that in Fig. 6b did not make any significant difference in computing the V_a because the ratio of these two fields is close to 1 over the most of North Pacific Ocean (Fig. 6e), revealing that the impact of water vapor in calculating C_D is small on the climatological time scales. However, there are differences when V_a is small, and this is consistent with the results shown in section 4. The reader should be cautioned that there could be impacts of water vapor on C_D on shorter time scales (e.g., daily or shorter), and this is especially true at low wind speeds and low relative humidities (see section 4).

Finally, Fig. 6f shows the land–sea mask used in the original 1.125° × 1.125° Gaussian grid for ERA-40 interpolated onto the 1/12° HYCOM domain. For example, a contour value of 0.6 implies that the wind stress magnitudes on the model grid are ≈60% contaminated by the wind stress magnitude over land. Some grids near the coast are represented as land points in ERA-40 but most of them should be ocean. Such problems in atmospheric forcing fields were also noted other studies (e.g., Metzger and Hurlburt 2001; Kara et al. 2005). Thus, it is clear that unrealistic wind stress magnitudes near such coastal region errors (see Fig. 6a) are largely due to the land–sea mask and orographically generated Gibb's waves. Gibb's waves are caused by the spectral truncation of the orography to triangular truncation (P. Kållberg, ECMWF, 2003, personal communication). When averaging fields originally created in the ERA-40's spectral geometry, traces of the originally minute Gibb's waves become more visible. For example, Metzger (2003) noted such atmospheric forcing problems in an ocean model study of the South China Sea. On the other hand, the atmospheric variables (e.g., T_a, u, v, etc) in the ERA-40 product are from postprocessed fields where the spectral traces have been removed, allowing one to calculate, for example, wind stress magnitude from these variables as we did in the North Pacific Ocean (Figs. 6b,c).

6. Summary and conclusions

Ocean models or coupled atmosphere–ocean models can be directly forced with net surface heat fluxes obtained from archived weather products. However, recalculating air–sea fluxes that are dependent upon the model SST is typically sufficient to keep model-simulated SSTs on track without any explicit relaxation to SST data or a climatology (although assimilation of SST data can further increase the model SST accuracy). This process requires reliable and efficient parameterizations of stability-dependent exchange coefficients over the global ocean, a topic that is investigated in this study.

We present simple and computationally efficient parameterizations of exchange coefficients for wind stress (C_D) and latent heat flux (C_L), which are of particular value not only for high-resolution global OGCM applications but also for various ocean mixed-layer and air–sea interaction studies. The polynomial functions for exchange coefficients are determined after running the COARE v3.0 algorithm for wind speed magnitudes at 10 m above the sea surface ranging from 1 to 40 m s^{-1}. The stability dependence in the exchange coefficients was accomplished by using air–sea temperature difference and air–sea mixing ratio difference through RH for a given wind speed at 10 m above the sea surface. It is shown that ignoring water vapor effects in the calculation of exchange coefficients can result in serious errors at low wind speeds, generally a serious underestimation of the exchange coefficients for $V_a < 5$ m s^{-1}. As an application of our methodology, climatological mean wind stress magnitude is calculated using 6-hourly meteorological variables from ERA-40 in the North Pacific Ocean over 1979–93. Such an analysis can identify possible problems existing in atmospheric forcing parameters (e.g., wind stress magnitude), which are directly output from coarse-resolution archived weather products (e.g., ERA-40) and demonstrates how these problems can be reduced using our methodology. The use of exchange coefficients from the polynomial functions in the wind stress bulk formulation not only reproduces wind stress magnitudes approximately comparable to the original ERA-40 field in the interior of the North Pacific Ocean, but also eliminates unrealistic and excessive noise near the land–sea boundaries that exist in the original ERA-40 field.

Finally, the motivation for this paper was to present sufficiently accurate transfer coefficients for air–sea

fluxes that were also computationally efficient enough to be used for climate model applications. Although the earlier COARE algorithm (v2.5b) required ≈20 iterations, the latest version (v3.0) iterates 3 times or less. However, even having three iterations at each time step would result in significant computational inefficiency for a fine resolution global OGCM that runs many years (e.g., decadal to interdecadal time scales). Exchange coefficients based on our derived polynomial functions can be calculated at ≈5 times lower computational cost than the more involved computations of COARE algorithm (v3.0) with three iterations for atmospheric stability. We also note here that the sensible heat flux coefficient C_S is assumed to be equal to C_L in this paper because, for simplicity, the roughness length for temperature is assumed equal to that for humidity in the algorithm. Further investigation concerning variable roughness lengths is beyond the scope of this study.

The exchange coefficients for air–sea fluxes presented in this paper are called the Naval Research Laboratory (NRL) Air–Sea Exchange Coefficients (NASEC). Two simple FORTRAN programs (one for C_D and one for C_L) along with the tabulated exchange coefficients based on various wind speed, relative humidity and air–sea temperature difference intervals can be downloaded from the Web site (available online at http://www7320.nrlssc.navy.mil/nasec/nasec.html).

Acknowledgments. The authors would like to extend special thanks to P. K. Taylor, Head of the James Rennell Division of the Southampton Oceanography Centre (SOC), for providing constructive criticisms to this paper. We appreciate the helpful comments of E. J. Metzger (NRL) during the preparation of this manuscript. We acknowledge the excellent comments of the two anonymous reviewers. This work is a contribution to the 6.2 project Hybrid Coordinate Ocean Model (HYCOM) and advanced data assimilation sponsored by the Office of Naval Research (ONR) under Program Element 602435N and to the project HYCOM consortium for data-assimilative ocean modeling sponsored under the National Ocean Partnership Program.

REFERENCES

Andreas, E. L, and K. A. Emanuel, 2001: Effects of sea spray on tropical cyclone intensity. *J. Atmos. Sci.,* **58,** 3741–3751.

Buck, A. L., 1981: New equations for computing vapor pressure and enhancement factor. *J. Appl. Meteor.,* **20,** 1527–1532.

Bunker, A. F., 1976: Computations of surface energy flux and annual air–sea interaction cycles of the North Atlantic Ocean. *Mon. Wea. Rev.,* **104,** 1122–1140.

DeCosmo, J., K. B. Katsaros, S. D. Smith, R. J. Anderson, W. A. Oast, K. Bumke, and H. Chadwick, 1996: Air–sea exchange of water vapor and sensible heat: The Humidity Exchange Over the Sea (HEXOS) results. *J. Geophys. Res.,* **101,** 12 001–12 016.

Emanuel, K., 2003: A similarity hypothesis for air–sea exchange at extreme wind speeds. *J. Atmos. Sci.,* **60,** 1420–1428.

Fairall, C. W., E. F. Bradley, D. P. Rogers, J. B. Edson, and G. S. Young, 1996: Bulk parameterization of air–sea fluxes for Tropical Ocean–Global Atmosphere Coupled–Ocean Atmosphere Response Experiment. *J. Geophys. Res.,* **101,** 3747–3764.

——, ——, J. E. Hare, A. A. Grachev, and J. B. Edson, 2003: Bulk parameterization of air–sea fluxes: Updates and verification for the COARE algorithm. *J. Climate,* **16,** 571–591.

Hare, J. E., P. O. G. Persson, C. W. Fairall, and J. B. Edson, 1999: Behavior of Charnock's relationship for high wind conditions. Preprints, *13th Symp. on Boundary Layers and Turbulence*, Dallas, TX, Amer. Meteor. Soc., 252–255.

Hurlburt, H. E., and P. J. Hogan, 2000: Impact of 1/8° to 1/64° resolution on Gulf Stream model-data comparisons in basin-scale subtropical Atlantic Ocean models. *Dyn. Atmos. Oceans,* **32,** 283–329.

Isemer, H.-J., J. Willebrand, and L. Hasse, 1989: Fine adjustment of large scale air– sea energy flux parameterizations by direct estimates of ocean heat transport. *J. Climate,* **2,** 1173–1184.

Janssen, J. A. M., 1997: Does wind stress depend on sea-state or not?—A statistical error analysis of HEXMAX data. *Bound.-Layer Meteor.,* **83,** 479–503.

Johnson, H. K., J. Hoejstrup, H. J. Vested, and S. E. Larsen, 1998: Dependence of sea surface roughness on wind waves. *J. Phys. Oceanogr.,* **28,** 1702–1716.

Kara, A. B., P. A. Rochford, and H. E. Hurlburt, 2000: Efficient and accurate bulk parameterizations of air–sea fluxes for use in general circulation models. *J. Atmos. Oceanic Technol.,* **17,** 1421–1438.

——, ——, and ——, 2002: Air–sea flux estimates and the 1997–1998 ENSO event. *Bound.-Layer Meteor.,* **103,** 439–458.

——, H. E. Hurlburt, P. A. Rochford, and J. J. O'Brien, 2004: The impact of water turbidity on the interannual sea surface temperature simulations in a layered global ocean model. *J. Phys. Oceanogr.,* **34,** 345–359.

——, A. J. Wallcraft, and H. E. Hurlburt, 2005: Sea surface temperature sensitivity to water turbidity from simulations of the turbid Black Sea using HYCOM. *J. Phys. Oceanogr.,* **35,** 33–54.

Keller, M. R., W. C. Keller, and W. J. Plant, 1992: A wave tank study of the dependence of X band cross sections on wind speed and water temperature. *J. Geophys. Res.,* **97,** 5771–5792.

Large, W. G., and S. Pond, 1981: Open ocean momentum flux measurements in moderate to strong winds. *J. Phys. Oceanogr.,* **11,** 324–336.

Lowe, P. R., 1977: An approximating polynomial for the computation of saturation vapor pressure. *J. Appl. Meteor.,* **16,** 100–103.

Metzger, E. J., 2003: Upper ocean sensitivity to wind forcing in the South China Sea. *J. Oceanogr.,* **59,** 783–798.

——, and H. E. Hurlburt, 2001: The importance of high resolution and accurate coastline geometry in modeling South China Sea inflow. *Geophys. Res. Lett.,* **28,** 1059–1062.

Oost, W. A., G. J. Komen, C. M. J. Jacobs, and C. van Oort, 2002:

New evidence for a relationship between wind stress and wave age from measurements during ASGAMAGE. *Bound.-Layer Meteor.,* **103,** 409–438.

Simmons, A. J., and J. K. Gibson, 2000: The ERA-40 project plan. ERA-40 Project Report Series, No. 1, 62 pp. [Available from ECMWF, Shinfield Park, Reading RG2 9AX, United Kingdom.]

Smith, S. D., 1988: Coefficients for sea surface wind stress, heat flux and wind profiles as a function of wind speed and temperature. *J. Geophys. Res.,* **93,** 15 467–15 472.

Taylor, P. K., and M. J. Yelland, 2001: The dependence of sea surface roughness on the height and steepness of the waves. *J. Phys. Oceanogr.,* **31,** 572–590.

——, and ——, 2003: Sea surface roughness: High winds and short fetches. Preprints, *83d AMS Annual Meeting,* Long Beach, CA, Amer. Meteor. Soc., CD-ROM, P3.5.

Wallcraft, A. J., A. B. Kara, H. E. Hurlburt, and P. A. Rochford, 2003: The NRL Layered Global Ocean Model (NLOM) with an embedded mixed layer submodel: Formulation and tuning. *J. Atmos. Oceanic Technol.,* **20,** 1601–1615.

Yelland, M. J., B. I. Moat, P. K. Taylor, R. W. Pascal, J. Hutchings, and V. C. Cornell, 1998: Wind stress measurements from the open ocean corrected for airflow distortion by the ship. *J. Phys. Oceanogr.,* **28,** 1511–1526.

——, ——, R. W. Pascal, and D. I. Berry, 2002: CFD model estimates of the airflow distortion over research ships and the impact on momentum flux measurements. *J. Atmos. Oceanic Technol.,* **19,** 1477–1499.